CrystEngComm

ROYAL SOCIETY OF CHEMISTRY

COMMUNICATION

View Article Online
View Journal | View Issue

Cite this: *CrystEngComm*, 2021, **23**, 268

Received 12th November 2020,
Accepted 7th December 2020

DOI: 10.1039/d0ce01640c

rsc.li/crystengcomm

Carbon (sp^3) tetrel bonding mediated BODIPY supramolecular assembly *via* unprecedented synergy of $C_{sp^3}\cdots N$ and $C_{sp^3}\cdots F$ pair interactions†

Mehmet Menaf Ayhan, *[a] Emrah Özcan,[ab] Burcu Dedeoglu, [a] Yurii Chumakov,[cd] Yunus Zorlu [a] and Bünyemin Coşut[a]

Here, we present the first example of sp^3 hybridized carbon centered (C_{sp^3}) tetrel bonding mediated 3D BODIPY assembly *via* the exceptional synergy of $C_{sp^3}\cdots N$ and $C_{sp^3}\cdots F$ pair interactions. The carbon tetrel bond interaction energies of $C_{sp^3}\cdots N$ and $C_{sp^3}\cdots F$ are amplified significantly as the size of the 1D chain grows from dimer to tetramer BODIPY units.

The significance of non-covalent interactions[1–5] between molecules has been well recognized in a wide range of fields including crystal engineering,[6] chemical reactions[7] and biological systems.[8] There are several types of non-covalent interactions that can be used as the driving force in the formation and stabilization of specific molecular and complex structures. While hydrogen bonding continues to be a dominant interaction,[9,10] there is a growing recognition that other nonconventional non-covalent interactions such as halogen,[11–13] tetrel,[14–16] pnictogen[17–19] and chalcogen[20–22] bonding can also be utilized to design and obtain desired aggregate structures. Among these interactions, tetrel bonding has been the subject of growing interest due to its significant role in chemical reactions[23,24] and biological systems.[25] Tetrel bonding can be defined as an attractive interaction between a positive electrostatic region (σ-hole) present on a tetrel atom and an electron donor such as a Lewis base, an anion or a radical.[26] The magnitude of the positive electrostatic potential of σ-holes depends on the polarizability of tetrel atoms and the electronegativity of neighboring atoms.[27]

Tetrel bonding is generally considered to be among the weakest interactions (chalcogen > halogen > pnicogen > tetrel).[28] However, this pattern does not follow the simple order of electronegativity of the central atom, which would have placed tetrel bonding as the strongest. This order is a result of the reduced approachability of the σ-holes in tetrels, where they are in the middle of three sp^3-hybridized bonds.[29] This low approachability reduces the tetrel bonding interaction energy by steric and repulsive electrostatic interactions. The heavier members of this group (Si, Ge, Sn, and Pb) can expand their valence to overcome this accessibility problem, whereas carbon cannot. Moreover, in most cases, the heavier tetrel atoms form stronger tetrel bonding due to their smaller electronegativity and larger polarization which place carbon as the weakest among them (C < Si < Ge < Sn < Pb).[30] Nevertheless, despite the weak nature of carbon based tetrel bonding, it is abundant in nature and its importance has been theoretically and experimentally validated for protein–ligand systems[31,32] and chemical reactions.[33] In addition, tetrel bonding, like most weak interactions, is known to exhibit non-additive cooperative effects, which means that the binding energy of a single molecule with a cluster is larger than that observed in a binary complex.[34–37]

The carbon tetrel bond can be formed with sp (C_{sp})-, sp^2 (C_{sp^2})- and sp^3 (C_{sp^3})-hybridized carbons in acetonitrile,[38,39] carbonyl,[40,41] carbon dioxide[42] and methyl groups,[43,44] respectively. Among these hybridized carbons, studies on C_{sp^3}-tetrel bonding, despite it being the most abundant in nature, are scarce and mainly based on small molecules and theoretical studies.[43–46]

Recent work from our group and others shows that control over supramolecular assembly of a complex structure like BODIPY and, as a result, control over its solid-state properties can be achieved with rational design of non-covalent interactions.[47–49] These studies disclosed that BODIPY can be a useful platform for the investigation of non-covalent interactions thanks to its rigidity, planar geometry and several sites which can be readily functionalized. Moreover, the BODIPY core contains four sterically accessible C_{sp^3}-atoms

[a] *Department of Chemistry, Gebze Technical University, Gebze, Kocaeli, Turkey. E-mail: menafayhan@gtu.edu.tr*
[b] *Institute of Physics, Faculty of Science, University of South Bohemia, Branišovská 1760, 370 05, České Budějovice, Czech Republic*
[c] *Department of Physics, Gebze Technical University, Gebze, Kocaeli, Turkey*
[d] *Institute of Applied Physics, MD-2028, Chisinau, Moldova*

† Electronic supplementary information (ESI) available: Complete synthetic and crystallographic details. CCDC 2011924–2011926. For ESI and crystallographic data in CIF or other electronic format see DOI: 10.1039/d0ce01640c

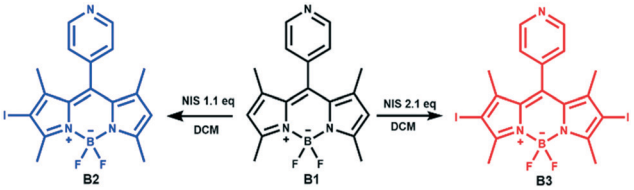

Fig. 1 Synthesis of **B1**, **B2** and **B3**.

($-CH_3$) which can be exploited as electrophilic sites to promote carbon tetrel bonding. To the best of our knowledge, we present here the first example of C_{sp^3} tetrel bonding mediated BODIPY assembly formed by anomalous synergistic $C_{sp^3}\cdots N$ and $C_{sp^3}\cdots F$ pair interactions (Fig. 1).

The iodination of meso-pyridyl BODIPY (**B1**) at the 2,6-positions yielded the corresponding iodo-BODIPY(**B2**) and diiodo-BODIPY (**B3**) derivatives with high yields and selectivity. The slow evaporation of solvents from the chloroform/hexane (1 : 2) mixture of **B1**, **B2** and **B3** yielded single crystals with centrosymmetric space groups *P*21/*c*, *P*21/*c* and *Cmcm*, respectively.

In **B1**, different non-classical C–H···F (dH···F = 2.59 Å) and C–H···N (dH···N = 2.61 Å) hydrogen bonding interactions link the molecules to construct a 2D layered hydrogen-bonded network (Fig. S11†), which further expanded into a 3D supramolecular network by C–H···N hydrogen bonds (dH···N = 2.70 Å) (Fig. S12†). In **B2**, the intermolecular C–H···F (dH···F = 2.43 to 2.49 Å) interactions form 1D infinite hydrogen bonded chains along the *c*-axis. These 1D chains are further expanded into a 3D supramolecular network by orthogonal oriented 1D chains generated through synergistic $C_{sp^3}\cdots N$ (3.247(6) Å) and $C_{sp^3}\cdots F$ (3.125(4) Å) pair interactions (Table S2 and Fig. 2D and S13†). In **B3**, F···π(BODIPY) interactions (2.695 Å) form a 1D chain structure along the *c*-axis, and these chains are connected through van der Waals dispersion interactions, containing short H···H (2.37 Å) contacts, to form a 2D layered structure (Fig. S14†).

It should be noted that upon formation of carbon tetrel bonding $C_{sp^3}\cdots X$ (N and F), there is geometrical deformation around the carbon atom, due to steric and repulsive electrostatic interactions, resulting from the movement of substituents to make more room for the Lewis base. This distortion was computed to be more energetically costly for smaller atoms, which is the reason behind the weak nature of the carbon tetrel bonding strength.[29,50] Therefore, in order to form efficient carbon tetrel bonding, the angle between C_{sp^3} and electron donors (N and F) must be high enough to geometrically expose the carbon atom. Single-crystal X-ray structure analysis revealed that the carbon tetrel bonding formation angle is 164.20° for $C_{sp^3}\cdots N$ and 162.59° for $C_{sp^3}\cdots F$ (Fig. 2C), which implies that the orientation of **B2** is driven by $C_{sp^3}\cdots X$ (N and F) interactions, and is not directed by a packing that minimizes steric hindrance.

The electrostatic surface potential (ESP)[51] map of **B2** was calculated and compared with those of **B1** and **B3** to serve as a reference point and to highlight the role of the electrostatic component in regulating the crystal packing of **B2**, shown in Fig. 3. In all cases, the potentials at the end of the pyridine and BF_2 groups are strongly negative. The electropositive regions are placed largely around the aromatic pyridine core and $-CH_3$ groups, where those close to pyridine exhibit a larger positive potential compared to those near the $-BF_2$ groups. The iodination of **B1** has led to the shift of negative potentials towards iodine atoms in **B2** and **B3**, whereas positive potentials of $-CH_3$ groups remained nearly the same for **B2** and slightly increased for **B3**. However, it may be noted that a specific σ-hole region on the carbon atom was not observed. Instead both carbon and hydrogen atoms in $-CH_3$ groups possess and share equal electropositive regions which should make either the carbon or the hydrogen

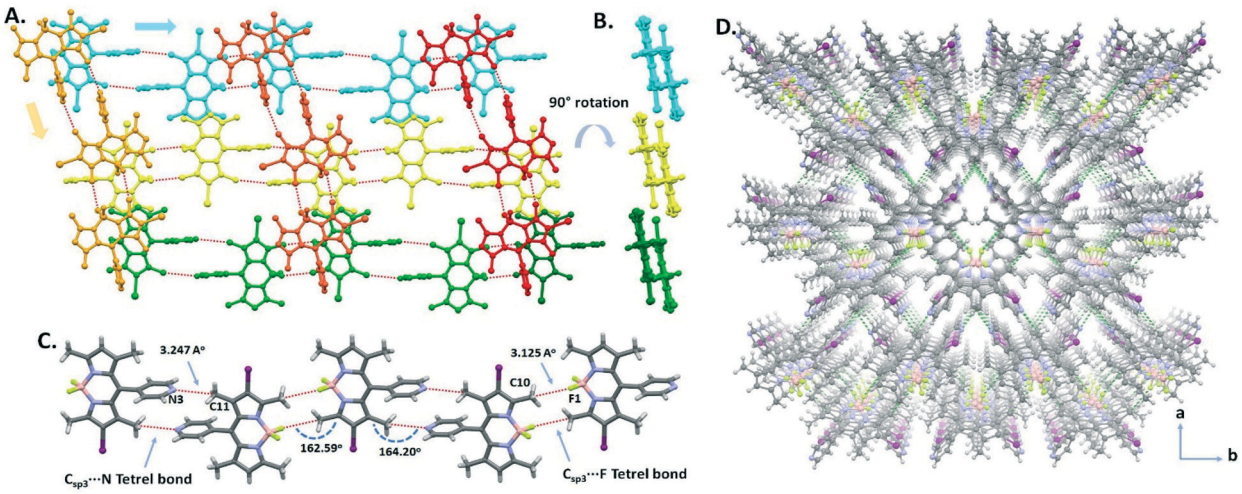

Fig. 2 (A) Perspective view of 1D carbon tetrel bonded infinite chains orthogonally oriented in crystal packing. (B) Front view of each carbon tetrel bonded chain by 90° rotation. (C) 1D infinite chains connected by homodimer $C_{sp^3}\cdots N$ and $C_{sp^3}\cdots F$ carbon tetrel bonding interactions. (D) Illustration of the 3D supramolecular network formed by F···H, $C_{sp^3}\cdots N$ and $C_{sp^3}\cdots F$ interactions.

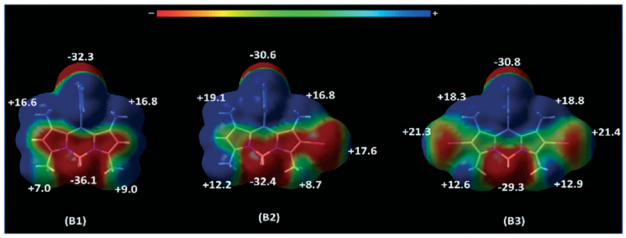

Fig. 3 The electrostatic surface potential (ESP) maps (kJ mol^{-1}) of **B1**, **B2** and **B3**.

bonding interactions equally favored, at least electrostatically, in all molecules. Furthermore, iodine atoms in **B2** and **B3** display large positive potential at the tip of their surface (σ-hole) which makes iodine a strong halogen bonding donating group and thus potentially leads to competitive halogen bonding in these molecules. Nevertheless, single-crystal X-ray structure analysis revealed that **B2** exhibits homodimer $C_{sp^3}\cdots N$ and $C_{sp^3}\cdots F$ carbon tetrel bond interactions but not hydrogen or halogen bonding which demonstrates the strength of cooperativity of carbon tetrel bond interactions.

The topological analysis of the electron density of the dimers has been carried out to gain insight into the pairwise $C_{sp^3}\cdots N$ and $C_{sp^3}\cdots F$ interactions using the AIM methodology (Table 1).[52] These analyses revealed the presence of a single intermolecular bond critical point (BCP) and its corresponding bond path between two molecules along the homodimer $C_{sp^3}\cdots N$ and $C_{sp^3}\cdots F$ contacts. The Laplacian of the electron density (P) at the BCP of both pairs of atoms is positive, identifying a depletion of the density between atoms. The positive value of the electronic energy density (H) at the BCP of the $C_{sp^3}\cdots N$ and $C_{sp^3}\cdots F$ contacts indicates the electrostatic character of such interactions. Furthermore, the potential energy density (V) calculation is used to estimate the binding energy for the $C_{sp^3}\cdots N$ and $C_{sp^3}\cdots F$ pair interactions, and the V values are equal to −9.999 and −9.137 kJ mol^{-1}, respectively (Table 1).

The symmetry adapted perturbation theory (SAPT)[53–56] analysis, which partitions the attractive energies into electrostatic (E_{elst}), exchange-repulsion (E_{exch}), induction (E_{ind}), and dispersion (E_{disp}) terms, has been carried out to unveil the nature of carbon tetrel bonds in **B2** and estimate their cooperativity effect. The cooperativity energy (E_{coop}) of trimer BODIPY, where molecules are joined by $C_{sp^3}\cdots N$ and $C_{sp^3}\cdots F$ tetrel bonds, was calculated to be the result of the interplay of these interactions: $E_{coop} = \Delta E_{1,2,3} - \Delta E_{1,2} - \Delta E_{2,3} - \Delta E_{1,3}$, where $\Delta E_{1,2,3}$ is the total interaction of the trimer ($\Delta E_{1,2,3} = E_{1,2,3} - 3E_1$), $\Delta E_{1,2}$ and $\Delta E_{2,3}$ are the interaction energies of the isolated dimers linked by $C_{sp^3}\cdots N$ and $C_{sp^3}\cdots F$ tetrel bonds, respectively, and the last term ($\Delta E_{1,3}$) is the interaction energy of molecules 1 and 3 in the geometry they have in the trimer (Fig. S15†). The computed cooperativity in terms of energy is found to be negative and equal to −7.681 kJ mol^{-1}, which indicates that the binding energy of the $C_{sp^3}\cdots N$ and $C_{sp^3}\cdots F$ tetrel bonds will be reinforced relative to the isolated binary complexes, as the size of the 1D chain grows.

The interaction energies (E_{int}) of homodimer $C_{sp^3}\cdots N$ and $C_{sp^3}\cdots F$ tetrel bonds are equal to −19.96 and −12.685 kJ mol^{-1}, respectively (Table 2). The dispersion forces are found to dominate in both non-covalent interactions, and in dimers, the absolute values of all attractive energy terms are greater for the $C_{sp^3}\cdots N$ tetrel bond than for the $C_{sp^3}\cdots F$ bond. Interestingly, as the chain grows from a dimer to a tetramer, the dispersion forces remain dominant; however there is a slight decrease for the $C_{sp^3}\cdots N$ interactions, while a significant increase for the $C_{sp^3}\cdots F$ interactions.

Moreover, unlike the dimers, all attractive energy terms are greater for the $C_{sp^3}\cdots F$ interaction than for the $C_{sp^3}\cdots N$ interaction in the tetramers (Fig. 4).

The interaction energies of the $C_{sp^3}\cdots N$ and $C_{sp^3}\cdots F$ tetrel bonds are amplified significantly, as the size of the 1D chain grows from a dimer to a tetramer, due to their impressive cooperative interactions (Table 2).

Additionally, the role of the exchange repulsive term significantly differs from dimer to tetramer formation. In the dimers the E_{exch} value for the $C_{sp^3}\cdots N$ tetrel bond is much higher than the E_{exch} value for $C_{sp^3}\cdots F$. However, in the tetramers, the E_{exch} value of the $C_{sp^3}\cdots N$ tetrel bond is decreased, whereas the E_{exch} value of the $C_{sp^3}\cdots F$ tetrel bond is increased significantly, probably due to the relatively smaller carbon tetrel bonding formation angle of $C_{sp^3}\cdots F$. Yet, these large E_{exch} energies were overcome by the amplified E_{elst}, E_{ind}, and E_{disp} attractive energy terms.

As the results indicate, the cooperativity effect based on the presence of $C_{sp^3}\cdots N$ tetrel bonds in the tetramer strengthens the binding energy of the $C_{sp^3}\cdots F$ interaction to an extraordinary level and continues to increase with growing chain length.

To conclude, we report here the first example of a carbon tetrel bonding mediated BODIPY assembly *via* homodimer $C_{sp^3}\cdots N$ and $C_{sp^3}\cdots F$ interactions resulting in an infinite 1D chain of **B2** in the crystal lattice. Our study shows that the cooperativity of the homodimer $C_{sp^3}\cdots N$ and $C_{sp^3}\cdots F$ interactions in terms of energy is very efficient and around

Table 1 Electron density ρ, Laplacian $\Delta\rho$ (a.u.), energy (H) and potential energy (V) density (kJ mol^{-1}) at the $C_{sp^3}\cdots X$ (N and F) tetrel bonds' critical points in dimers

$C_{sp^3}\cdots X$	P	$\Delta\rho$	H	V
$C_{sp^3}\cdots N$	0.007	0.025	3.2	−9.999
$C_{sp^3}\cdots F$	0.005	0.026	4.038	−9.137

Table 2 Summary of the SAPT results (kJ mol^{-1}) for the dimers and tetramers (in bold)

$C_{sp^3}\cdots X$	E_{elst}	E_{exch}	E_{ind}	E_{disp}	E_{int}	E_{coop}
$C_{sp^3}\cdots N$	−12.50	23.88	−3.29	−28.05	−19.96	**−7.68**
	−13.79	**17.72**	**−4.40**	**−24.89**	**−25.35**	
$C_{sp^3}\cdots F$	−6.98	8.86	−2.19	−12.37	−12.69	
	−24.86	**47.84**	**−6.64**	**−56.28**	**−39.95**	

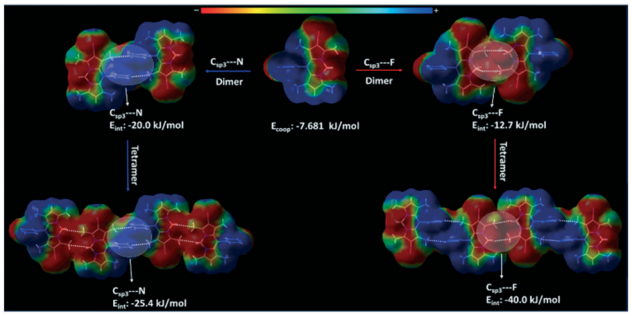

Fig. 4 The electrostatic surface potential (ESP) maps of the monomer, dimers and tetramers of **B2** and their E_{int} $C_{sp^3}\cdots X$ (N, F) values in kJ mol^{-1} calculated by SAPT.

−7.681 kJ mol^{-1} in the trimer BODIPY units. The carbon tetrel bond interaction energy amplified impressively for both the $C_{sp^3}\cdots N$ and $C_{sp^3}\cdots F$ interactions in the tetramer compared to the dimer BODIPY units. These results demonstrate that sp^3 hybridized carbon tetrel-bonding interactions can indeed be used for supramolecular engineering of complex structures like BODIPY. Thus, considering the abundance of $-CH_3$ groups in synthetic and natural organic molecules, their potential applications will greatly extend to numerous molecular disciplines, *e.g.*, supramolecular chemistry, crystal engineering, chemical reactions and biological systems.

The authors thank the TUBITAK ULAKBIM High Performance and Grid Computing Center (TRUBA resources), Turkey, for computational facilities.

Conflicts of interest

There are no conflicts to declare.

Notes and references

1 M.-D. K. Hobza Pavel, *Non-Covalent Interactions: Theory and Experiment*, Royal Society of Chemistry, 2009.
2 S. Scheiner, *Noncovalent Forces*, Springer International Publishing, 2015.
3 A. M. Maharramov, K. T. Mahmudov, M. N. Kopylovich and A. J. L. Pombeiro, *Non-covalent Interactions in the Synthesis and Design of New Compounds*, Wiley, 2016.
4 K. T. Mahmudov, A. V. Gurbanov, M. F. C. Guedes da Silva and A. J. L. Pombeiro, *Noncovalent Interactions in Catalysis*, Royal Society of Chemistry, 2019.
5 A. Bauzá, T. J. Mooibroek and A. Frontera, *ChemPhysChem*, 2015, **16**, 2496–2517.
6 C. Solids, S. Mandal, T. K. Mukhopadhyay, N. Mandal and A. Datta, *Cryst. Growth Des.*, 2019, **19**, 4802–4809.
7 M. Raynal, P. Ballester, A. Vidal-ferran and P. W. N. M. Van Leeuwen, *Chem. Soc. Rev.*, 2014, **43**, 1660–1733.
8 F. De Leo, A. Magistrato and D. Bonifazi, *Chem. Soc. Rev.*, 2015, **44**, 6916–6953.
9 P. Tholen, C. A. Peeples, R. Schaper, C. Bayraktar, T. S. Erkal, M. M. Ayhan, B. Çoşut, J. Beckmann, A. O. Yazaydin, M. Wark, G. Hanna, Y. Zorlu and G. Yücesan, *Nat. Commun.*, 2020, **11**, 1–7.
10 G. Gilli and P. Gilli, *The Nature of the Hydrogen Bond*, Oxford Scholarship Online, 2009.
11 Ö. D. Ateş, Y. Zorlu, S. D. Kanmazalp, Y. Chumakov, A. G. Gürek and M. M. Ayhan, *CrystEngComm*, 2018, **20**, 3858–3867.
12 P. Metrangolo and G. Resnati, *Halogen Bonding*, Springer International Publishing, 2008.
13 G. Cavallo, P. Metrangolo, R. Milani, T. Pilati, A. Priimagi, G. Resnati and G. Terraneo, *Chem. Rev.*, 2016, **116**, 2478–2601.
14 A. Bauzá, T. J. Mooibroek and A. Frontera, *Angew. Chem., Int. Ed.*, 2013, **52**, 12317–12321.
15 A. Bauzá, S. K. Seth and A. Frontera, *Coord. Chem. Rev.*, 2019, **384**, 107–125.
16 A. Daolio, P. Scilabra, G. Terraneo and G. Resnati, *Coord. Chem. Rev.*, 2020, **413**, 213265.
17 S. Scheiner, *Acc. Chem. Res.*, 2013, **46**, 280–288.
18 K. T. Mahmudov, A. V. Gurbanov, V. A. Aliyeva, G. Resnati and A. J. L. Pombeiro, *Coord. Chem. Rev.*, 2020, **418**, 213381.
19 S. Zahn, R. Frank, E. Hey-Hawkins and B. Kirchner, *Chem. – Eur. J.*, 2011, **17**, 6034–6038.
20 D. J. Pascoe, K. B. Ling and S. L. Cockroft, *J. Am. Chem. Soc.*, 2017, **139**, 15160–15167.
21 P. Scilabra, G. Terraneo and G. Resnati, *Acc. Chem. Res.*, 2019, **52**, 1313–1324.
22 K. T. Mahmudov, M. N. Kopylovich, M. F. C. Guedes Da Silva and A. J. L. Pombeiro, *Dalton Trans.*, 2017, **46**, 10121–10138.
23 S. C. A. H. Pierrefixe, J. Poater, C. Im and F. M. Bickelhaupt, *Chem. – Eur. J.*, 2008, **14**, 6901–6911.
24 J. K. R. Deka, B. Sahariah, K. Baruah, A. K. Bar and B. K. Sarma, *Chem. Commun.*, 2020, **56**, 4874–4877.
25 Á. M. Montaña, *ChemistrySelect*, 2017, **2**, 9094–9112.
26 A. Bauzá, T. J. Mooibroek and A. Frontera, *Chem. Rec.*, 2016, **16**, 473–487.
27 M. Hou, K. Jin, Q. Li and S. Liu, *RSC Adv.*, 2019, **9**, 18459–18466.
28 W. Dong, Q. Li and S. Scheiner, *Molecules*, 2018, **23**, 1–17.
29 E. Solel and S. Kozuch, *Molecules*, 2018, **23**, 2742–2749.
30 S. Scheiner, *J. Phys. Chem. A*, 2017, **121**, 5561–5568.
31 V. R. Mundlapati, D. K. Sahoo, S. Bhaumik, S. Jena, A. Chandrakar and H. S. Biswal, *Angew. Chem., Int. Ed.*, 2018, **57**, 16496–16500.
32 X. García-Llinás, A. Bauzá, S. K. Seth and A. Frontera, *J. Phys. Chem. A*, 2017, **121**, 5371–5376.
33 A. Karim, N. Schulz, H. Andersson, B. Nekoueishahraki, A. C. C. Carlsson, D. Sarabi, A. Valkonen, K. Rissanen, J. Gräfenstein, S. Keller and M. Erdélyi, *J. Am. Chem. Soc.*, 2018, **140**, 17571–17579.
34 I. Alkorta, M. M. Montero-Campillo, O. Mó, J. Elguero and M. Yáñez, *J. Phys. Chem. A*, 2019, **123**, 7124–7132.
35 M. Marín-Luna, I. Alkorta and J. Elguero, *J. Phys. Chem. A*, 2016, **120**, 648–656.
36 A. S. Mahadevi and G. N. Sastry, *Chem. Rev.*, 2016, **116**, 2775–2825.

37 J. George and R. Dronskowski, *J. Phys. Chem. A*, 2017, **121**, 1381–1387.
38 A. R. van der Werve, Y. R. Van Dijk and T. J. Mooibroek, *Chem. Commun.*, 2018, **54**, 10742–10745.
39 V. D. P. N. Nziko and S. Scheiner, *Phys. Chem. Chem. Phys.*, 2016, **18**, 3581–3590.
40 R. Shukla and D. Chopra, *CrystEngComm*, 2018, **20**, 3308–3312.
41 M. T. Doppert, H. Van Overeem and T. J. Mooibroek, *Chem. Commun.*, 2018, **54**, 12049–12052.
42 I. Alkorta, J. Elguero and J. E. Del Bene, *J. Phys. Chem. A*, 2017, **121**, 8017–8025.
43 V. L. Heywood, T. P. J. Alford, J. J. Roeleveld, S. J. Lekanne Deprez, A. Verhoofstad, J. I. van der Vlugt, S. R. Domingos, M. Schnell, A. P. Davis and T. J. Mooibroek, *Chem. Sci.*, 2020, **11**, 5289–5293.
44 T. J. Mooibroek, J. J. Roeleveld, S. J. Lekanne Deprez, A. Verhoofstad, A. Frontera and J. I. van der Vlugt, *Chem. – Eur. J.*, 2020, **26**, 1–8.
45 S. P. Thomas, M. S. Pavan and T. N. Guru Row, *Chem. Commun.*, 2014, **50**, 49–51.
46 A. Bauzá, T. J. Mooibroek and A. Frontera, *Chem. Commun.*, 2014, **50**, 12626–12629.
47 E. Özcan, B. Dedeoglu, Y. Chumakov, A. G. Gürek, Y. Zorlu, B. Coşut and M. M. Ayhan, *Chem. – Eur. J.*, 2020, DOI: 10.1002/chem.202003945.
48 M. Su, X. Yan, X. Guo, Q. Li, Y. Zhang and C. Li, *Chem. – Eur. J.*, 2020, **26**, 4505–4509.
49 H. Hassanain, E. S. Davies, W. Lewis, D. L. Kays and N. R. Champness, *Crystals*, 2020, **10**, 1–11.
50 S. Scheiner, *J. Phys. Chem. A*, 2018, **122**, 2550–2562.
51 L. C. Gilday, S. W. Robinson, T. A. Barendt, M. J. Langton, B. R. Mullaney and P. D. Beer, *Chem. Rev.*, 2015, **115**, 7118–7195.
52 M. A. Spackman, *Chem. Phys. Lett.*, 1999, **301**, 425–429.
53 B. Jeziorski, R. Moszynski and K. Szalewicz, *Chem. Rev.*, 1994, **94**, 1887–1930.
54 T. Korona, R. Moszynski and B. Jeziorski, *J. Chem. Phys.*, 1996, **105**, 8178–8186.
55 K. Szalewicz, *Wiley Interdiscip. Rev.: Comput. Mol. Sci.*, 2012, **2**, 254–272.
56 J. M. Turney, A. C. Simmonett, R. M. Parrish, E. G. Hohenstein, F. A. Evangelista, J. T. Fermann, B. J. Mintz, L. A. Burns, J. J. Wilke, M. L. Abrams, N. J. Russ, M. L. Leininger, C. L. Janssen, E. T. Seidl, W. D. Allen, H. F. Schaefer, R. A. King, E. F. Valeev, C. D. Sherrill and T. D. Crawford, *Wiley Interdiscip. Rev.: Comput. Mol. Sci.*, 2012, **2**, 556–565.

